THE JOURNAL OF BIOLOGICAL CHEMISTRY VOL. 291, NO. 29, pp. 15057–15068, July 15, 2016

New Insight into the Catalytic Mechanism of Bacterial MraY from Enzyme Kinetics and Docking Studies*

Received for publication, January 26, 2016, and in revised form, May 16, 2016 Published, JBC Papers in Press, May 18, 2016, DOI 10.1074/jbc.M116.717884

Yao Liu (刘垚)[‡1], João P. G. L. M. Rodrigues[§], Alexandre M. J. J. Bonvin[§], Esther A. Zaal[¶], Celia R. Berkers[¶2], Michal Heger[‖], Katarzyna Gawarecka[**], Ewa Swiezewska[**], Eefjan Breukink[‡3], and Maarten R. Egmond[‡]

*From [‡]Institute of Biomembranes, Department of Membrane Biochemistry and Biophysics, Utrecht University, 3584 CH, Utrecht, the Netherlands, the Departments of [§]Computational Structural Biology and [¶]Biomolecular Mass Spectrometry and Proteomics, Bijvoet Center for Biomolecular Research, Utrecht University, 3584 CH, Utrecht, the Netherlands, the [‖]Department of Experimental Surgery, Academic Medical Center, University of Amsterdam, 1105 AZ, Amsterdam, The Netherlands, and the **Institute of Biochemistry and Biophysics, Polish Academy of Sciences, 02-106 Warsaw, Poland*

Phospho-MurNAc-pentapeptide translocase (MraY) catalyzes the synthesis of Lipid I, a bacterial peptidoglycan precursor. As such, MraY is essential for bacterial survival and therefore is an ideal target for developing novel antibiotics. However, the understanding of its catalytic mechanism, despite the recently determined crystal structure, remains limited. In the present study, the kinetic properties of *Bacillus subtilis* MraY (BsMraY) were investigated by fluorescence enhancement using dansylated UDP-MurNAc-pentapeptide and heptaprenyl phosphate (C35-P, short-chain homolog of undecaprenyl phosphate, the endogenous substrate of MraY) as second substrate. Varying the concentrations of both of these substrates and fitting the kinetics data to two-substrate models showed that the concomitant binding of both UDP-MurNAc-pentapeptide-DNS and C35-P to the enzyme is required before the release of the two products, Lipid I and UMP. We built a model of BsMraY and performed docking studies with the substrate C35-P to further deepen our understanding of how MraY accommodates this lipid substrate. Based on these modeling studies, a novel catalytic role was put forward for a fully conserved histidine residue in MraY (His-289 in BsMraY), which has been experimentally confirmed to be essential for MraY activity. Using the current model of BsMraY, we propose that a small conformational change is necessary to relocate the His-289 residue, such that the translocase reaction can proceed via a nucleophilic attack of the phosphate moiety of C35-P on bound UDP-MurNAc-pentapeptide.

Among the enzymes involved in bacterial peptidoglycan synthesis, phospho-*N*-acetylmuramyl-pentapeptide translocase (MraY[4]; EC 2.7.8.13) has been studied extensively (1, 2). This enzyme performs the initial membrane step in this process, forming undecaprenyl-*N*-acetylmuramyl-pentapeptide (Lipid I) from UDP-*N*-acetylmuramyl-pentapeptide (UDP-MurNAc-pentapeptide) and undecaprenyl phosphate, in both Gram-positive and Gram-negative bacteria. Given the role of MraY in bacterial cell wall synthesis (3, 4) and cell growth (5), this enzyme is an interesting target for antibacterial drugs. Recently, the crystal structure of MraY from the Gram-negative species *Aquifex aeolicus* (Protein Data Bank entry 4J72) was determined (6). The enzyme was extracted from its membrane environment with detergent and crystallized as a symmetrical homodimer. Each protomer consists of 10 transmembrane helices, with both the N and C termini locating on the periplasmic side (outside) of the cytoplasmic membrane (1). Before the publication of this high resolution (3.3 Å) structure, other studies attempted to unravel the catalytic mechanism of action of MraY by site-directed mutagenesis and kinetics studies, using either membrane-embedded MraY or detergent-extracted and purified preparations (1, 7, 8). These studies proposed that catalysis proceeds most likely via a one-step process, although a two-step process has also been suggested (1). In the single-step process, a ternary complex of MraY, UDP-MurNAc-pentapeptide, and undecaprenyl phosphate (C55-P) yields Lipid I with concomitant release of UMP. In the two-step process, UMP is released, yielding a covalently bound phospho-MurNAc-pentapeptide intermediate that is subsequently attacked by C55-P to produce Lipid I. However, no direct experimental evidence was provided for either proposal. The kinetics values of MraY for its nucleotide and lipid substrates that have been reported in literature so far are not consistent with each other. Bouhss *et al.* (7) obtained the K_m value of MraY by varying the concentration of one substrate while keeping the other at a fixed value. The authors reported apparent K_m values for UDP-MurNAc-pentapeptide and C55-P of 1.0 ± 0.3 and 0.16 ± 0.08 mM, respectively. This result was later challenged by another study (9) reporting an apparent K_m value for UDP-MurNAc-pentapeptide at 36.2 ± 3.6 μM. The major difference between these two studies is the concentration of C55-P used in the reaction, namely 1.1 mM (7) and 50 μM (9). This indicates that the concentration of both substrates should be varied to allow determination of the true K_m value. In the present study, we performed more extensive kinetics studies on the detergent-solubilized MraY. Pure heptaprenyl phosphate (C35-P) was used as the preferred lipid substrate throughout our study.

* The authors declare that they have no conflicts of interest with the contents of this article.

[1] Supported by ZonMW Grant 205.100.008 from the Netherlands Organization for Scientific Research (NWO).
[2] Supported by a VENI grant (project 722.013.009) from the NWO.

[3] To whom correspondence should be addressed: Membrane Biochemistry and Biophysics, Institute of Biomembranes, Utrecht University, 3584 CH, Utrecht, the Netherlands. Tel.: 31-30-2533523; E-mail: E.J.Breukink@uu.nl.

[4] The abbreviations used are: MraY, phospho-MurNAc-pentapeptide translocase; BsMraY, *Bacillus subtilis* MraY; AaMraY, *Aquifex aeolicus* MraY; UDP-MurNAc-pentapeptide or UMpp, UDP-*N*-acetylmuramic acid-pentapeptide; C35-P, heptaprenyl phosphate; C55-P, undecaprenyl phosphate; DDM, *N*-dodecyl-β-D-maltopyranoside; [$^{15}N_2$]UMP, uridine-[$^{15}N_2$]5′-monophosphate; TM, transmembrane helix.

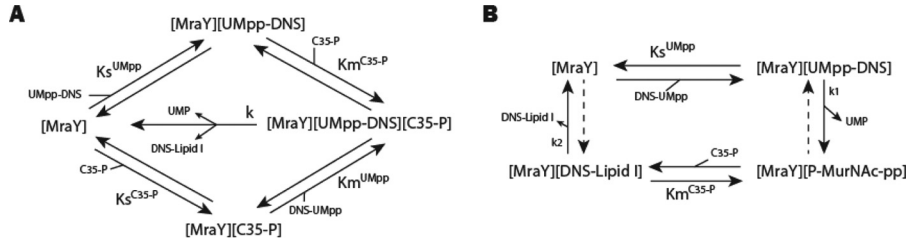

FIGURE 1. **Kinetic models used to derive the rate equations for the MraY-catalyzed reaction.** *A*, random bi-bi kinetic mechanism, in which MraY binds in a random order to its two substrates; the two products will only be released after a ternary complex is formed between MraY and its substrates. In this model, the substrates bind to the same enzyme species. *B*, ping-pong mechanism, in which one of the substrates binds first, and a first product is formed. The second substrate therefore binds to a modified enzyme species, and a second product is then released.

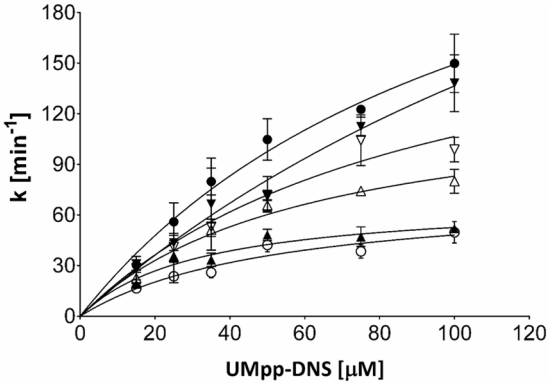

FIGURE 2. **Turnover of DNS-Lipid I formation (*k*) as a function of UDP-MurNAc-pentapeptide-DNS concentration and at several concentrations of C35-P (20 μM (○), 35 μM (▲), 50 μM (△), 100 μM (▽), 200 μM (▼), and 400 μM (●)).** *Error bars*, S.E.

Other MraY studies (10, 11) have also reported the use of C35-P instead of the natural lipid substrate C55-P. Polyprenyl phosphates with shorter chain lengths are also accepted as substrates by MraY (12), but to the best of our knowledge, the exact effect of the prenyl chain length on the activity of MraY has not yet been studied in detail. Together with kinetic studies, we built a model for MraY from *Bacillus subtilis*, carried out docking experiments with C35-P, and analyzed the conserved residues in both Gram-positive and Gram-negative MraY species. The shortened chain length of C35-P compared with C55-P makes the docking results more reliable because of the reduced number of possible conformations of the prenyl chain. Many algorithms/programs are available for predicting protein-substrate binding. The majority of these approaches, however, focus on soluble proteins in an aqueous environment because more experimental data are available. For our docking studies, HADDOCK (high ambiguity driven protein-protein docking) (13), an approach developed for protein complex docking based on biochemical and/or biophysical interaction data, was used. Unlike other docking methods, HADDOCK uses ambiguous interaction restraints to drive the docking. The docked structures are given a HADDOCK score, after calculations, according to their intermolecular energy, namely a weighted sum of desolvation, van der Waals, electrostatic, and ambiguous interaction restraint energy terms. In our case, the default desolvation energy term for aqueous protein docking was neglected, and a novel "*z*-restraint" was introduced to keep our model in the right orientation in the simulated membranes. Together, our findings provided a novel concept for the development of MraY inhibitors and imply that blocking the binding of the lipid substrate to the enzyme, by targeting His-298, may be a viable approach. This is of great interest, given that the inhibitor development for MraY has not been very successful so far.

Results

N-Dodecyl-β-D-maltopyranoside (DDM)-BsMraY Kinetics—To understand the catalytic mechanism of MraY and how its activity is controlled, it is important to consider the binding of both substrates to the enzyme and thus vary both of their concentrations during the kinetics studies. This has been previously neglected in kinetic analysis of MraY activity (7, 9). The kinetics of BsMraY extracted from the *Escherichia coli* membrane with 1% DDM detergent were investigated by varying both substrates, C35-P and UDP-MurNAc-pentapeptide-DNS, yielding a dansylated product DNS-Lipid I and UMP. Production of DNS-Lipid I was monitored using fluorescence enhancement measurements (14). Immediately after the addition of enzyme, the fluorescence signal increased linearly for several minutes. The reaction was followed until a plateau was reached. This plateau value was then used to convert the fluorescence signal into concentration of DNS-Lipid I. Slopes obtained from the linear part of the reaction traces could then be expressed in μM/min of Lipid I formed. These values were finally divided by the concentration of MraY to obtain reaction rates k (min^{-1}). Reaction rates were collected using a range of concentrations of one substrate while maintaining the concentration of the other constant. The experiments were repeated at least three times for six concentrations of both UDP-MurNAc-pentapeptide-DNS and C35-P. All experimental data were fitted to the equations for either a two-substrate model (Fig. 1*A*) or ping-pong mechanism (Fig. 1*B*). Better fit was obtained for a random bi-bi model (SSE (sum of squared errors of prediction) = 8330.1, RMSE (root mean square error) = 9.2) than for a ping-pong model (SSE = 8655.3, RMSE = 9.4), indicating that a ternary complex is formed between the enzyme, UDP-MurNAc-pentapeptide-DNS, and C35-P.

When the data as shown in Fig. 2 were fitted separately at constant C35-P concentrations, an apparent maximum turnover $k_{cat(app)}$ and K_{mapp}^{UMpp} were obtained at the various levels of C35-P used. Replotting these apparent parameters as a function of C35-P (Fig. 3) yielded the maximum turnover (k_{cat}) and the true K_m values for C35-P and UDP-MurNAc-pentapeptide-DNS, and $K_s^{C35\text{-}P}$. The dependent variable K_s^{UMpp} was calculated from the other three constants. In Table 1, the results are summarized.

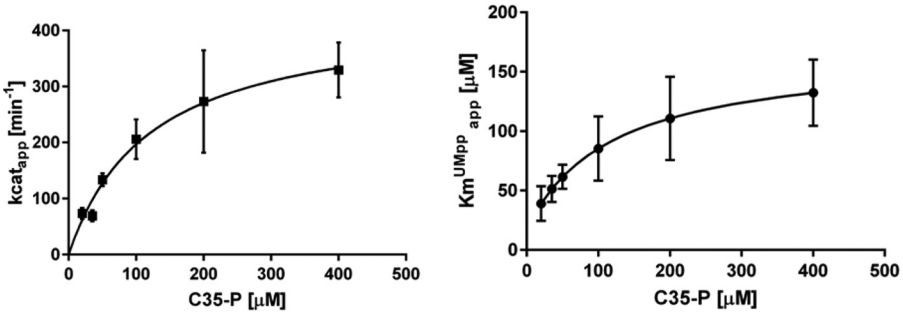

FIGURE 3. **Replots of $k_{cat(app)}$ (■; *left*) and K_{mapp}^{UMpp} (●; *right*) as a function of C35-P concentration.** The apparent turnover rate increases as C35-P concentration increases, and the binding affinity of UDP-MurNAc-pentapeptide to MraY decreases. *Error bars*, S.E.

TABLE 1
Kinetic parameters obtained for BsMraY

K_m^{UMpp}	$K_m^{C35\text{-}P}$	K_s^{UMpp}	$K_s^{C35\text{-}P}$	k_{cat}
μM	μM	μM	μM	min^{-1}
167 ± 18	121 ± 23	18 ± 31	13 ± 11	434 ± 35

These data show that K_m for either substrate increases by 1 order of magnitude when a ternary complex is formed compared with binding of either substrate in binary complex formation.

Exchange between UDP-MurNAc-Pentapeptide and Uridine-[$^{15}N_2$]5′-Monophosphate ([$^{15}N_2$]UMP)—The choice of the random bi-bi mechanism for MraY catalysis, based on better fitting data, could be supported by a mass spectrometry-based experiment devised to detect exchange between [$^{15}N_2$]UMP and UDP-MurNAc-pentapeptide either in the absence or presence of C35-P. In such an experiment, the exchange reaction will result in the formation of unlabeled $^{14}N_2$-UMP from unlabeled UDP-MurNAc-pentapeptide, resulting in a mass difference in UMP of ~2 Da that can be detected by LC-MS analysis. At the same time, the reverse reaction will catalyze the transfer of [$^{15}N_2$]uridine from uridine-[$^{15}N_2$]5′-monophosphate to UDP-MurNAc-pentapeptide, resulting in the formation of [$^{15}N_2$]UDP-MurNAc-pentapeptide. To investigate under which conditions exchange occurred, UDP-MurNAc-pentapeptide (100 μM) and [$^{15}N_2$]UMP (1 mM) were incubated with DDM-BsMraY in the absence or presence of C35-P for 16 h. Given that the major difference between the two models is the requirement of polyprenyl phosphate for the hydrolysis of UDP-MurNAc-pentapeptide and formation of Lipid I, the reaction was performed using pure enzyme devoid of C55-P instead of enzyme-containing membranes where C55-P was still present. It should also be noted that incubations were carried out with a 10-fold higher concentration of [$^{15}N_2$]UMP relative to unlabeled UDP-MurNAc-pentapeptide to clearly observe the reverse reaction and the formation of ^{15}N-labeled UDP-MurNAc-pentapeptide. After removal of the detergent, the resulting reaction mixture was analyzed by LC-MS. It was found that in the absence of C35-P, no $^{14}N_2$-UMP was produced, and no $^{15}N_2$ was transferred from UMP to UDP-MurNAc-pentapeptide. However, in the presence of 100 μM C35-P, both $^{14}N_2$-UMP and [$^{15}N_2$]UDP-MurNAc-pentapeptide were found in the mixture, as shown in Fig. 4. This clearly demonstrates that an exchange between UMP and UDP-MurNAc-pentapeptide happens only when C35-P is available.

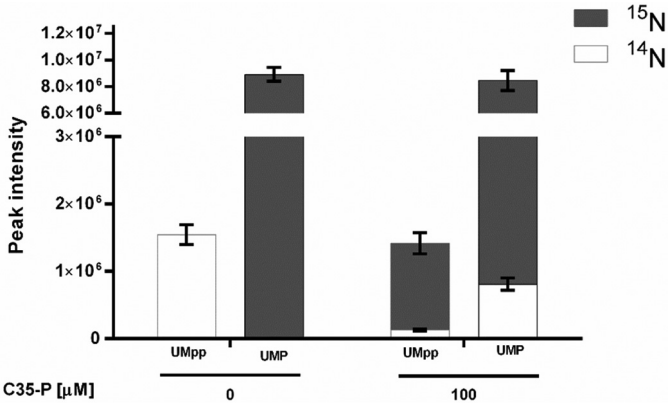

FIGURE 4. **LC-MS analysis of the products of a reaction mixture containing MraY, $^{14}N_2$-UDP-MurNAc-pentapeptide, and [$^{15}N_2$]UMP in the absence and presence of C35-P.** Two *groups* of *columns* are shown for these two different conditions of the assay. In the *left group*, where C35-P is absent, only $^{14}N_2$-UDP-MurNAc-pentapeptide and [$^{15}N_2$]UDP-MurNAc-pentapeptide were detected. In the *right group*, where 100 μM C35-P was included, [$^{15}N_2$]UDP-MurNAc-pentapeptide and $^{14}N_2$-UDP were detected as a result of an exchange reaction. *Error bars*, S.E.

Structural Model of BsMraY—Given the results from the aforementioned kinetics and exploration of the exchange reaction, a structure would be very helpful in giving more insight into the catalytic mechanism of BsMraY. Because there is no crystal structure of BsMraY available, we built a homology model based on the structure of MraY from *A. aeolicus*. Protein sequence databases contain over 5000 MraY sequences (PFam PF10555 and IPR018480). Following a BLAST search, aligning the sequences of MraY of both Gram-positive and Gram-negative species reveals that more than 50 amino acids are fully retained in these two families. Based on sequence analysis, AaMraY and BsMraY are good representatives of all Gram-negative and Gram-positive MraY families, respectively. Given the lack of structure for BsMraY (Uniprot ID: Q03521), we produced a model based on the available AaMraY structure. Only a small region of the model is considered "poorly modeled," corresponding to the disordered loop region of BsMraY (residues 30–53) that does not exist in *A. aeolicus* MraY and that does not make part of our predicted interface with C35-P (see "Identity and Location of Conserved Residues"). The best-ranked model, according to the DOPE statistical potential implemented in MODELLER, is shown in Fig. 5 together with the structure of AaMraY. The models are viewed from the plane of the membrane, as calculated by the PPM2.0 server (15). Two short α-helices are present in Gram-negative MraY species

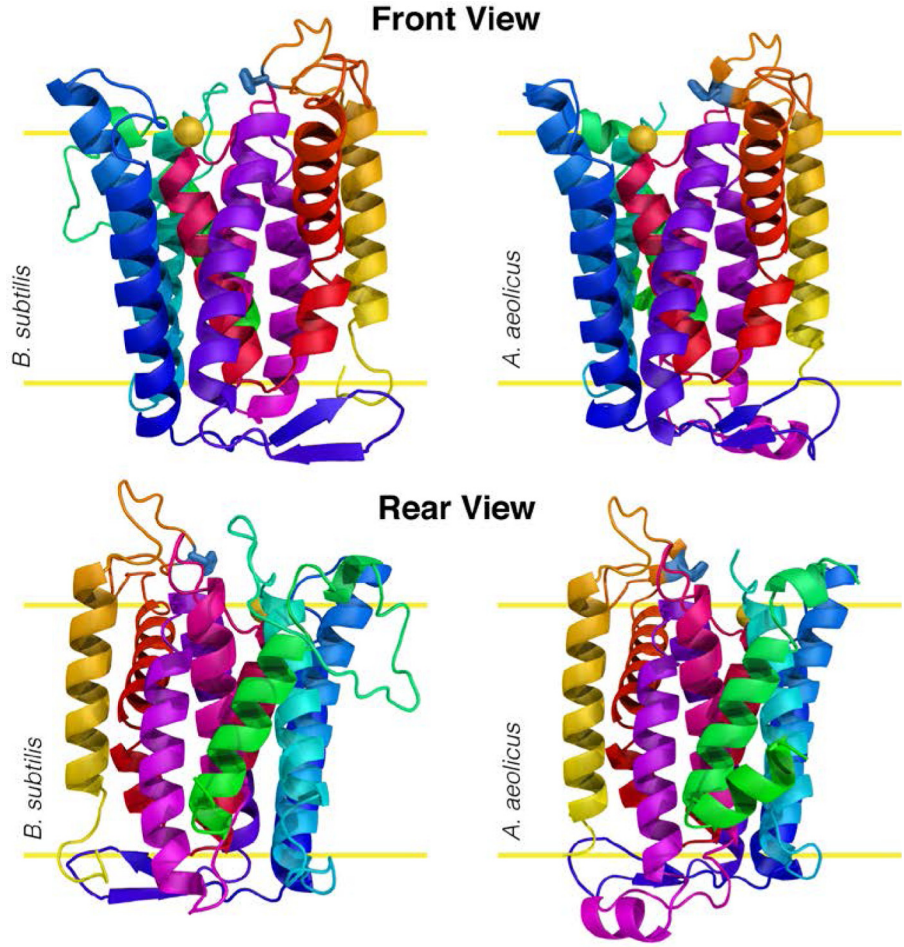

FIGURE 5. **Structural models of BsMraY (*left*) and AaMraY (*right*).** The structures are viewed from the plane of the membrane: cytoplasmic (inside) and periplasmic (outside) regions at the *top* and *bottom*, respectively. The membrane is represented by the *yellow lines* and placed as calculated by the PPM2.0 server. Both structures are *colored* from *green* (N terminus) to *yellow* (C terminus), with the catalytic Mg^{2+} represented as a *gold sphere* and His-289 (*B. subtilis*) and His-324 (*A. aeolicus*) in *blue sticks*. The two transmembrane helices central to the modeling studies, TM5 and TM9, are *colored purple* and *dark red*, respectively, in both structures. The *back view* highlights the differences between the two structures, namely two α-helices (in *magenta* on the cytoplasmic side and in *green* at the N terminus) that are present only in MraY from Gram-negative species.

only. One of these is present at the N terminus of MraY from *A. aeolicus* and is proposed to align with the surface of the membrane (6), whereas the other is found between TM6 and TM7 and located in the periplasm.

Two transmembrane helices, TM5 and TM9, in *purple* and *dark red* in Fig. 5, respectively, are relevant for this study in particular. There are no significant differences between the predicted lengths and orientations of these helices in the BsMraY model when compared with the structure of AaMraY; TM9 is strongly twisted, whereas TM5 is slanted relative to the other transmembrane helices, giving rise to a nearly perpendicular orientation of TM5 with respect to the C-terminal part of TM9. The transmembrane helix TM5 points toward the highly conserved His-324 in AaMraY or His-289 in BsMraY, shown in *blue sticks* in Fig. 5. This histidine residue was shown to be catalytically important, but no clear role had been attributed to this residue (7, 16). We also observed that the mutant H289R is virtually inactive in both the TLC-based Lipid II synthesis assay and the Lipid I synthesis-based fluorescence enhancement assay (data not shown).

Identity and Location of Conserved Residues—All conserved amino acids, grouped with respect to their properties, are listed in Table 2 along with their location in the protein structure of BsMraY. With the exception of Glu-251 and Lys/Arg-249, all residues are located at the cytosolic side of MraY quite close to the Mg^{2+} ion (average distance 11 $\pm$ 5 Å). For the highly conserved His-45, no reliable structural data are available (the corresponding His-67 coordinates are missing in Protein Data Bank entry 4J72). Residues that are not retained in MraY species from plants are marked with an asterisk. When the analysis is expanded to include the functionally related proteins TarO, TagO, RgpG, WbpL, WbcO, and WecA, one finds some 20 fully conserved amino acids. These residues are shown in boldface type in Table 2. The fully conserved His-289 is at a distance of 8.4 Å from the Mg^{2+} ion. Apart from being close to Mg^{2+}, several conserved residues are close together in space, most likely for structural reasons (*e.g.* Phe-228 in the loop between TM7 and TM8 with Gly-178 and Asp-174 in TM5). It should be noted that the conserved Lys-102 residue is located very close to Mg^{2+} but is replaced by Ile in *Staphylococcus aureus* MraY.

Docking of C35-P to the Model of BsMraY—Because no crystal structure of BsMraY with its lipid substrate is available, we attempted to predict the binding mode of BsMraY to C35-P through docking studies. Inspection of the BsMraY models sug-

gested that flexibility might play a role in substrate binding, in particular the orientation of TM9. Given the limited ability of HADDOCK to sample large conformational changes, we used CONCOORD to generate additional conformers of BsMraY. These conformers were then used to seed new docking calculations using the same parameters and restraints as before. Indeed, after correcting for the disordered and poorly modeled loops in the BsMraY model, CONCOORD hints that the highest flexibility in MraY is found at the C-terminal tip of TM9 and part of the connecting residues between TM9 and TM10 (residues ~271–285). This part of MraY is highly positively charged due to the presence of four or five Lys and/or Arg residues, depending on different MraY species, of which Lys/Arg-276, Arg-281, and Lys/Arg-284 are fully conserved (Table 2). The N-terminal part of TM9 is much less flexible, probably helped by the proximity of the conserved Lys-249 and Glu-251 residues. High flexibility, but to a lesser extent, was found in the loop connecting TM3 and TM4. In this loop, at the C-terminal end of TM3 and the N-terminal end of TM4, again many Lys and/or Arg residues are located, of which Lys/Arg-114 and Lys-116 are highly conserved (Table 2).

The docking studies yielded nine possible binding modes for C35-P (see Table 3). All models are consistent in that MraY seems to fully accommodate only seven isoprene units of the polyprenyl phosphates. This predicts that the lipid tail of natural polyprenyl phosphates containing 11 isoprene units, as in C55-P, will not bind completely to MraY. The clusters differ mainly in the conformation of C35-P and consequent interactions that it makes with MraY residues and its coordinated magnesium ion. Clusters 6, 4, 7, and 9 have very shallow interfaces and are unlikely to represent realistic binding modes, as indicated by their low HADDOCK score. Clusters 5 and 8, despite being the top scoring clusters, do not show any significant interactions between the phosphate moiety and any MraY residues and have therefore been discarded from subsequent analyses. Clusters 2 (*blue* in Fig. 6) and 1 favor interactions with the magnesium coordination center and the ion itself, whereas cluster 3 (*green* in Fig. 6) shows a binding mode where the phosphate of C35-P is in close proximity with His-289 (*dark pink* in Fig. 6), which may indicate that this residue is important for the interaction with the phosphate and would explain the loss of activity upon modification of this residue (see more details under "Discussion"). In cluster 3, the entire C35-P molecule is in an extended conformation along TM5, also in proximity with highly conserved residues of TM9 (Glu-264, Ser-267, Val-268, and Gln-271). In the remaining clusters, C35-P shows a kink near the phosphate group. The several clusters also select different conformers of MraY, in particular of TM9, indicating that there might be a conformational mechanism involving transmembrane helix reorientation to better accommodate the ligand.

TABLE 2

Conserved residues in MraY family

Residue numbering is given for BsMraY. Lys-102 is replaced by Ile in *S. aureus* MraY. The location of each residue is listed: TM, transmembrane helix. Loops between transmembrane helices are indicated by the numbers of the two flanking helices. The shortest distances to Mg^{2+} ion are shown for all residues. For residue His-45 (−) structural data are lacking. Shown in boldface are residues that are also retained in related proteins. Shown in italic type residues within 10Å of the Mg^{2+} ion. *, residues that are not retained in MraY from plant species. Hydrophobic residues are shaded.

Location	Residue	Dist. (Å) Mg^{2+}	Location	Residue	Dist. (Å) Mg^{2+}	Location	Residue	Dist. (Å) Mg^{2+}
1-2	H45(b)	-	5-6	*L172**	7.1	8-9	K/R249*	28.6
	K48(b)	21.5		T173	10.7	TM9	E251* (a)	24.5
TM2	***P52***	8.8		***D174*** (a)	5.3		E264 (a)	14.7
	T53	6.2		***G175***	5.5		S267	16.5
	M54	12.2		*L176*	7.2		V268	12.4
	G55	14.5		***D177*** (a)	10		Q271	15.1
	G56	12		***G178***	9.9	9-10	K/R276* (b)	18.7
TM3	G92*	12	TM7	G216	21		R281	17.7
	G95	7.4		F217	14.3		F283	19.4
	D98 (a)	5.1		**N221**	15.2		K/R284 (b)	21.1
	D99 (a)	6.1	7-8	P224	19.7		P287	12
TM4	*K102** (b)	3.4		A225	17.4		***H289*** (b)	8.4
3-4	K106 (b)	14		*F228**	7.4		H290 (b)	12.4
	G110	8.5		*M229*	8.3		H291 (b)	15.4
TM4	**K/R114** (b)	13.1	TM8	***G230***	5.5		E292* (a)	19.3
	*K116** (b)	4.1		***D231*** (a)	2.1		E299 (a)	20.2
TM5	**N168**	10.5		***G233***	7.9			
	A169*	10.3		*L235*	6.8			
	N171	3.2		**G238**	12.1			

Discussion

Kinetics of Detergent-solubilized BsMraY—BsMraY was chosen as a representative phospho-MurNAc-pentapeptide translocase from Gram-positive species due to its robust properties, although structural information was lacking. In contrast to *E. coli* MraY, BsMraY shows high activity after resolubilization in detergent systems (9). Similar to other MraY studies (10, 11), pure C35-P was used as the lipid substrate in our kinetics studies to be consistent with our docking studies. Interestingly, it was previously found that at least 35 carbon units were required for the polyprenyl phosphate to be a substrate of WecA, an

TABLE 3

Statistics of scoring and relevant distances for each cluster after explicit solvent refinement

All values are averages and S.D. calculated from the best scoring four models of each cluster. Distances to the C35-P are reported from the phosphorous atom. *z*-score, standard score; vdW, van der Waals; Elec, electrostatic; AIRs, ambiguous interaction restraints; BSA, buried surface area.

Cluster	HADDOCK score	*z*-Score	Size	Energy terms			BSA	Distances to C35-P		
				vdW	Elec	AIRs		Mg	His-289	Asp-98
				kcal/mol			*Å²*		*Å*	
5	−51 ± 3	−1.2	18	−48 ± 10	−114 ± 18	2.6 ± 1	1253 ± 59	7.6 ± 2.6	15.1 ± 1.5	5.9 ± 1.8
2	−47 ± 6	−1.1	98	−39 ± 5	−141 ± 23	18 ± 15	1224 ± 69	3.1 ± 0.2	10.9 ± 2.3	5.2 ± 1.2
8	−39 ± 12	−0.8	7	−50 ± 4	−87 ± 20	4 ± 2	1264 ± 35	9.3 ± 0.9	14.3 ± 2.8	5.8 ± 2.1
1	−35 ± 1	−0.6	169	−34 ± 3	−104 ± 19	18 ± 17	1037 ± 25	5.5 ± 1.9	10.3 ± 2.4	6.3 ± 1.3
3	−28 ± 4	−0.3	47	−35 ± 2	−45 ± 10	31 ± 31	1118 ± 39	10.1 ± 1.4	4.2 ± 1.6	14.0 ± 2.5
6	−10 ± 7	0.5	13	−26 ± 3	−60 ± 32	8 ± 10	906 ± 91	9.1 ± 0.9	13.0 ± 2.8	11.4 ± 2.0
4	−9 ± 7	0.5	24	−21 ± 1	−44 ± 55	34 ± 17	848 ± 39	7.3 ± 2.3	7.2 ± 1.3	10.5 ± 1.9
7	14 ± 7	1.4	9	−19 ± 3	−78 ± 26	72 ± 23	665 ± 128	12.8 ± 2.2	16.3 ± 1.7	12.4 ± 3.1
9	18 ± 11	1.6	4	−20 ± 6	−62 ± 28	95 ± 16	703 ± 135	13.0 ± 1.9	16.9 ± 2.3	10.8 ± 1.6

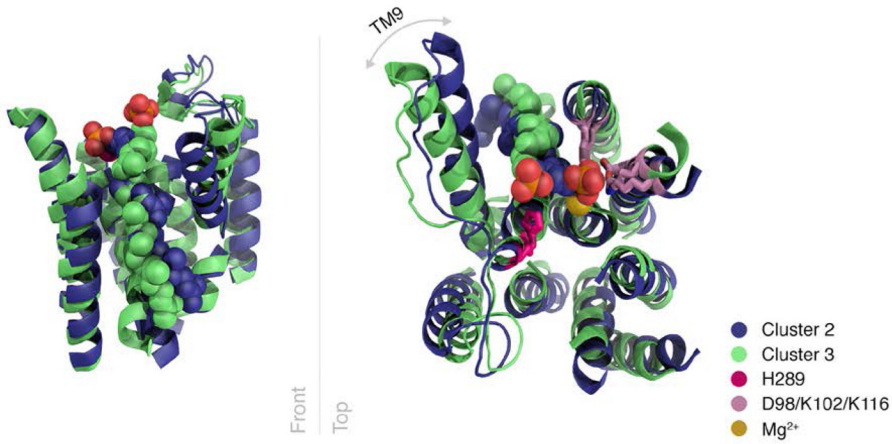

FIGURE 6. **Different binding modes of C35-P to BsMraY suggested by the modeling.** *Left*, *side view* of the binding modes of clusters 2 (*blue*) and 3 (*green*). *Right*, *top view* of the same clusters, highlighting important residues (*sticks*, *light pink*) near the phospho-binding site. Interhelical loops are omitted for clarity, except for those containing His-289 (*sticks*, *dark pink*). The *red*/*orange spheres* represent the oxygen and phosphorous atoms of the phosphate group of C35-P, whereas the *gold spheres* represent magnesium ions.

enzyme that is functionally similar to MraY (17). Our kinetics studies using fluorescence enhancement show that the apparent affinity for UDP-MurNAc-pentapeptide depends on the concentration of C35-P and *vice versa*. This means that the concomitant binding of UDP-MurNAc-pentapeptide and C35-P forming a ternary complex with MraY occurs before liberation of the products Lipid I and UMP. Furthermore, it was shown that binding affinities for UDP-MurNAc-pentapeptide and C35-P are relatively low (*i.e.* K_m values are in the high micromolar range for either substrate when a ternary complex is formed). In contrast, the binding affinities for single substrate binding are much higher. These affinities could not be determined accurately but are about 1 order of magnitude higher than the corresponding affinities in ternary complex formation. In summary, the kinetics study supports models in which ternary complexes between MraY and the two substrates are formed but clustering of the two substrates makes it harder for either substrate to bind in the presence of the other substrate than to bind to MraY alone. This indicates that in the ternary complex formed during catalysis, the two substrates bind closely together to allow the reaction to occur without the need for a covalently bound substrate-MraY intermediate.

In previous kinetic studies on BsMraY using radioactively labeled UDP-MurNAc-pentapeptide (*e.g.* Bouhss *et al.* (7, 8)), only affinities for either substrate were obtained in the presence of fixed (saturating) concentrations of the other. Compared with our studies, the turnover of MraY found ($320 \pm 25\ min^{-1}$) is close to our result ($434 \pm 35\ min^{-1}$). The K_m found by us for UDP-MurNAc-pentapeptide (0.167 ± 0.018 mM) is lower than the value reported (0.94 ± 0.15 mM). Interestingly, although the polyprenyl substrate used (C55-P) differed from ours (C35-P), the K_m values are quite close: 0.16 ± 0.04 mM for C55-P (7) and 0.12 ± 0.02 mM for C35-P (see also "Docking of Polyprenyl Phosphate"). In other kinetic studies, a very low K_m value for UDP-MurNAc-pentapeptide (19 μM) was reported (10, 18). We only observed such a high affinity ($K_s^{UMpp} = 18\ \mu M$) for UDP-MurNAc-pentapeptide binding to MraY when the concentration of C35-P was extrapolated to zero (see Fig. 3 or Table 1). We propose, therefore, that a high apparent affinity for UDP-MurNAc-pentapeptide will be observed when the translocase is not saturated with the polyprenyl phosphate substrate. This can be verified by quantifying the amount of Lipid I formed under the conditions used.

Docking of Polyprenyl Phosphate—Chung *et al.* (6) proposed a mode of binding of C55-P where the phosphate moiety of C55-P is located close to Asp-117 (Asp-98 in BsMraY) of AaMraY. In addition, they predicted the polyprenyl chain to bend sharply, in order to allow such a location for the phosphate. Although the authors confirmed that His-324 (His-289 in BsMraY) is involved in catalysis, no catalytic role was attributed to this highly conserved histidine residue. In our docking studies, the only (initial) assumptions made were the likelihood (based on an initial unbiased docking run) of the polyprenyl tail of C35-P to bind along TM5 in MraY and the directionality of the C35-P substrate. In all four best scoring binding modes, C35-P was bound in a kinked fashion in the isoprene chain near the phosphate moiety. Furthermore, in these modes, the phosphate is found close to Asp-98 with its OH hydrogen pointing toward the carboxylate oxygens of Asp-98. Because we were unable to dock the other substrate, UDP-MurNAc-pentapeptide, as well, it remains to be established whether the binding modes for polyprenyl phosphates near Asp-98 would be affected by the other substrate. Close inspection of the models predicts that in principle, there is room for the diphosphate of UDP-MurNAc-pentapeptide to bind in the neighborhood of the catalytic Mg^{2+} ion, even when C35-P binds closely to Asp-98 and the Mg^{2+} ion. In the fifth best scoring cluster, C35-P is bound in an extended fashion, where the phosphate moiety is located very close to the aromatic ring of His-289. This suggests a direct involvement of His-289 in the transfer of the phosphate moiety of polyprenyl phosphate as described below. It should be noted that docking of C55-P was complicated because of the parameterization and flexibility of this molecule. Our activity test indicated that the longer chain of C55-P does not contribute to or improve binding to MraY (data not shown).

Catalytic Role of His-289—Our docking studies hint at two possible scenarios in which His-289 is involved in the catalytic

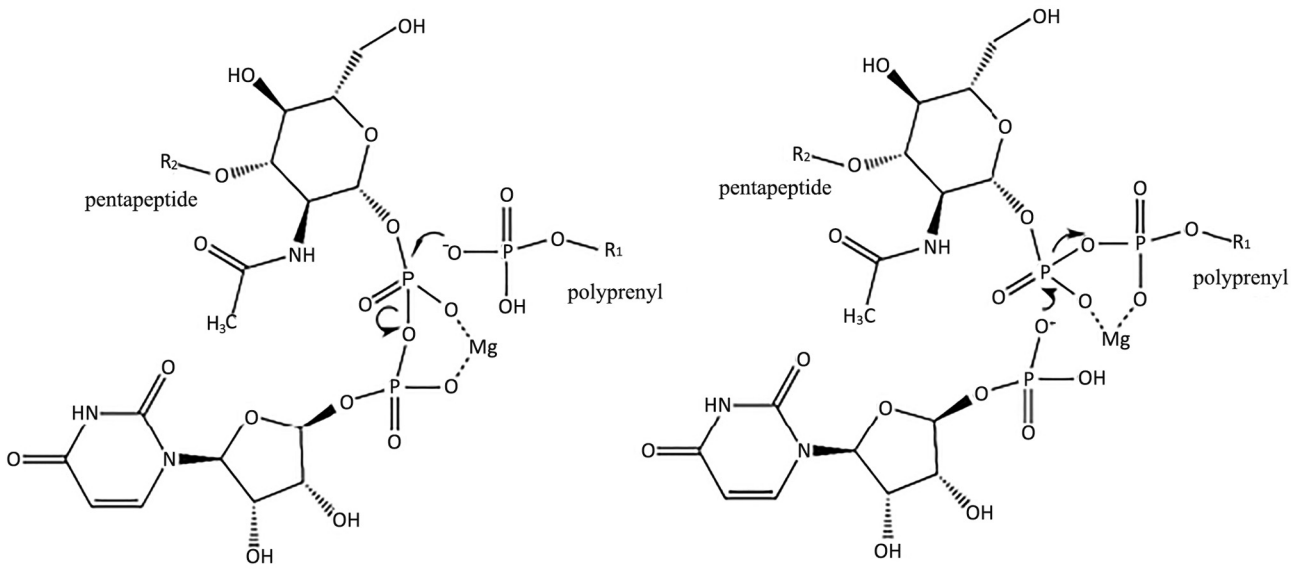

FIGURE 7. **Concerted S_N2 type mechanism of transferase reactions catalyzed by MraY; deprotonation of the phosphate moiety of polyprenyl phosphate allows subsequent nucleophilic attack on bound UDP-MurNAc-pentapeptide.**

mechanism of MraY (*i.e.* by binding to the phosphate moiety of the C35-P forming a phosphoramidate bond between one of the nitrogen atoms and the phosphorous atom of the polyprenyl phosphate substrate). Alternatively, His-289 may act as a base, thereby activating the phosphate for reaction with UDP-MurNAc-pentapeptide. In either scenario, a small conformational change (involving TM9) will be needed to bring the phosphate moiety a few Å closer to the catalytic Mg^{2+} ion, thereby kinking the isoprene chain as we observed for clusters 5, 2, 8, and 6 (Fig. 6, *right*). In the event that a covalent bond is formed, dephosphorylation of His-289 can be catalyzed by nearby acidic groups, such as Asp-174, after the conformational change. Using our kinetic analysis, we tried to verify the finding of Al-Dabbagh *et al.* (8) that the mutation H289R apparently does not affect the affinities for UDP-MurNAc-pentapeptide and C55-P while lowering catalytic turnover by 5 orders of magnitude. It turned out, however, that no reliable affinities could be obtained, due to the very high enzyme concentration needed (~400 μM) to observe turnover (data not shown). Under these conditions, the steady state assumption used in Michaelis-Menten kinetics no longer applies, and hence the calculation of K_m is invalid. Such a catalytic role of His-289 as depicted above is comparable with the involvement of a histidine residue in the activity of undecaprenyl pyrophosphate phosphatase UppP from *E. coli* (19). The catalytic histidine in UppP was proposed to act either as a base or by forming a phosphoramidate bond with undecaprenyl pyrophosphate, similar to our proposal. It should be noted, however, that MraY is not able to break the pyrophosphate bond in undecaprenyl pyrophosphate, most likely because the pyrophosphate moiety cannot be accommodated properly in the active site of the enzyme. Furthermore, the pyrophosphate moiety present in UDP-MurNAc-pentapeptide cannot be hydrolyzed by MraY in the absence of polyprenyl phosphate. MS analysis only showed exchange of ^{14}N and ^{15}N isotopes between UMP and UDP-MurNAc-pentapeptide in the presence of C35-P, as was suggested by previous studies using radiolabeled UMP (8). This result is also in line with our finding that both substrates UDP-MurNAc-pentapeptide and C35-P need to bind before the products Lipid I and UMP are liberated. However, it contradicts the formation of phospho-MurNAc-pentapeptide from UDP-MurNAc-pentapeptide, as has been postulated before (20).

The involvement of conformational changes in MraY translocase activity has been suggested before based on inhibition studies (1, 21, 22). The lysis protein E from bacteriophage ΦX174 strongly inhibits MraY from Gram-negative species. Residues present in TM9 were found to be implicated in protein E binding (23). However, MraY from Gram-positive species are not affected by protein E. Although a conformational change similar to that proposed in, for example, MraY from *E. coli* might still occur in the enzymes from Gram-positive species, this could not be verified using protein E, because BsMraY does not bind to protein E strongly if at all (23).

Reaction Mechanism—The translocase activity of MraY requires clustering of the two substrates, UDP-MurNAc-pentapeptide from solvent water and polyprenyl phosphate with its hydrophobic tail embedded in the membrane environment. Based on the crystal structure of MraY from *A. aeolicus*, Chung *et al.* (6) proposed a reaction mechanism, where Asp-98 (Asp-117 in Protein Data Bank entry 4J72) is involved in deprotonation of the phosphate moiety of polyprenyl phosphate, allowing subsequent nucleophilic attack on bound UDP-MurNAc-pentapeptide (*e.g.* as shown in Fig. 7). Alternatively, or in addition, activation of the phosphate moiety of polypropylene phosphate may proceed involving His-289. When the reaction proceeds according to the mechanism shown, the oxyanion of polyprenyl phosphate performs a nucleophilic attack on the phosphate moiety of MurNAc-pentapeptide, leading to the formation of Lipid I. Concomitantly, the phosphorus–oxygen bond between UMP and the phosphate moiety of MurNAc pentapeptide is broken. This S_N2 type process is fully reversible, providing a basis for the observed reaction, where incubations with UMP and Lipid I give rise to UDP-MurNAc-pentapeptide and polyprenyl phosphate.

Alternative reaction mechanisms have been proposed where the translocase reaction proceeds via a nucleophilic attack on UDP-MurNAc-pentapeptide by an acidic residue in MraY (1) (*e.g.* Asp-98). In this process, UMP will be liberated in a similar fashion as shown in Fig. 7. A covalently bound phospho-MurNAc-pentapeptide intermediate will then be formed, either yielding Lipid I after reaction with polyprenyl phosphate or reproducing UDP-MurNAc-pentapeptide in the presence of high concentrations of UMP. It was found, however, that in the absence of C35-P, MraY did not catalyze a nucleotide exchange process between UDP-MurNAc-pentapeptide and UMP (Fig. 4). Our work strongly suggests that polyprenyl phosphate is needed to activate MraY. This means that the alternative scenario, in which the reaction proceeds via a nucleophilic attack on UDP-MurNAc-pentapeptide by an acidic residue in the enzyme, is less likely than a direct attack of polyprenyl phosphate on UDP-MurNAc-pentapeptide yielding Lipid I and UMP, as illustrated in Fig. 7. When Lipid I is bound to the enzyme, MraY may still reside in its activated form such that activation of UMP is not required for the nucleophilic attack on bound Lipid I, yielding UDP-MurNAc-pentapeptide and polyprenyl phosphate. It remains to be established in detail how the essential histidine His-289 is catalytically involved in the translocase activity of MraY. It is clear, however, that His-289 is not simply involved in binding of either substrate. More likely, it is needed to activate the phosphate moiety of the polyprenyl phosphate. In this process, a (slight) conformational change in MraY is essentially required for catalysis yielding Lipid I. Whether or not His-289 is also catalytically required in the reverse reaction between Lipid I and UMP remains to be established as well.

Inhibition of Translocase Activity—The kinetics and docking study presented here have given new insight into the mechanism underlying MraY catalysis. Although MraY has long been considered an ideal target for novel antimicrobial compounds, the inhibitor development for this enzyme has so far not been very successful. Most studies on inhibition of MraY to eventually block peptidoglycan synthesis have been focused on competitive inhibition by UDP-MurNAc-pentapeptide analogs, such as tunicamycin (24). Our current work provides structural insight into how to possibly block MraY activity by focusing on the polyprenyl phosphate substrate; a promising approach would be to specifically alkylate or covalently block the essential histidine in the enzyme (His-289 in BsMraY) using, for example, a competitive inhibitor that mimics the polyprenyl substrate.

In addition, the noncompetitive inhibition of MraY from Gram-negative species by protein E has been reported (11, 22, 23). Protein E inhibition of MraY is probably attributable to locking the enzyme in an inactive configuration such that conformational change cannot take place. Although protein E is found to be inactive against Gram-positive MraY, the structural homology of Gram-negative and Gram-positive MraY is such that conformational changes needed to activate the enzyme are very likely to be similar. If, indeed, the inhibition from E is due to locking MraY in a form such that no accommodation of the hydrophobic polyprenyl phosphate could occur, screening for similar inhibitors that will also bind to Gram-positive species will widen the scope for such an inhibition mechanism.

Experimental Procedures

Materials—Unless stated otherwise, all chemicals used were purchased from Sigma-Aldrich. All DNA ladders, restriction enzymes, and buffers were purchased from Thermo Fisher Scientific. Oligonucleotides (primers) for DNA amplification (PCRs) and sequencing were synthesized by Integrated DNA Technologies (Leuven, Belgium). Sequencing services for all DNA constructs were provided by Macrogen (Amsterdam, The Netherlands). pET28a vector was purchased from Merck Millipore (Amsterdam, The Netherlands). EDTA-free protease inhibitor mixture tablets were obtained from Roche Diagnostics (Risch-Rotkreuz, Switzerland). DDM was obtained from Affymetrix (Santa Clara, CA). Precision Plus Protein™ standards were purchased from Bio-Rad. Isopropyl-β-D-thiogalactopyranoside was purchased from Thermo Fisher Scientific. ΔSlyD BL21 (DE3) *E. coli* strain was a kind gift from Prof. Ry Young (Texas A&M University, College Station, TX). LysC protease was purchased from Wako Pure Chemical Industries (Osaka, Japan). Heptaprenol (C35-) and undecaprenol (C55-) were isolated and then phosphorylated to C35-P and C55-P, respectively, as described previously (25, 26).

Recombinant Wild Type MraY—A DNA fragment coding for BsMraY protein was amplified from *B. subtilis* 168 by colony PCR using the following primers: BamHI-BY, 5′-ggatccatgcttgagcaagtcattcgtttac-3′; BY-HindIII, 5′-aagctttataaccacacctcg-3′. The restriction sites are underlined. Standard protocols were used for PCR amplification, digestion, ligation into pET28a vector, recombinant plasmid transformation, and propagation. The resulting expression plasmid was named pET28a-BsY, which carries an N-terminal His_6 tag, a thrombin cleavage site, and a T7 tag. The sequence was confirmed by sequencing analysis (Macrogen).

H289R-BsMraY—Site-directed mutagenesis was performed on pET28aBsY to generate the single mutant H289R using primers H289R-for (5′-ctttaaaatgagtccgcttcgtcaccattatgagcttgtc-3′) and H289R-rev (5′-gacaagctcataatggtgacgaagcggacttattttaaag-3′). The mismatch for arginine coding is underlined. The protocol is based on one used previously (27) with construct-specific modifications. Briefly, PCR was performed using Phusion polymerase with an annealing temperature of 72 °C for 50 s and plasmid elongation at 72 °C for 6 min. DpnI (0.25 μl, 20 units/μl) was added to the PCR mixture and incubated at 37 °C for 1 h before transformation. Plasmid isolation was performed subsequently using the Qiagen MiniPrep kit. The resulting sequence was confirmed by sequencing analysis (Macrogen).

Protein Purification—For protein expression, we used an *E. coli* strain that has a deletion in the *slyD* gene to prevent contamination of the purified MraY with this protein. For each preparation, pET28aBsY and mutant were freshly transformed into competent Δ*slyD* BL21(DE3) *E. coli* cells and subsequently inoculated into Luria broth (1% tryptone, 0.5% yeast extract, and 1% NaCl) supplemented with kanamycin (50 μg/ml) for overnight growth at 37 °C. This preculture was diluted the next day at a ratio of 1:100 into prewarmed (37 °C) Terrific broth (1.2% tryptone, 2.4% yeast extract, 0.4% glycerol, 17 mM KH_2PO_4, 72 mM K_2HPO_4) supplemented with kanamycin (50 μg/ml). The growth was continued at 37 °C up to an $A_{600\ nm}$

of ~0.5. Subsequently, isopropyl-β-D-thiogalactopyranoside (final concentration = 100 μM) was added to induce protein expression. The growth was continued at 22 °C for 4 h. For each batch of purified MraY, 5 liters of cells expressing BsMraY or its mutant were harvested and disrupted by probe sonication. The membrane was subsequently solubilized by the addition of 1% DDM in buffer A (25 mM Tris-HCl (pH 7.6), 150 mM NaCl, 10% glycerol). The mixture was centrifuged at 206,000 × *g* for 45 min. The supernatant was collected, and 1% DDM was added to the pellet for a second round of solubilization. The solubilized membrane protein fractions were pooled and incubated with Ni^{+}-NTA-agarose beads pre-equilibrated with buffer A supplemented with 20 mM imidazole. Beads loaded with protein were subsequently transferred to a gravity column for batch-wise IMAC purification. Pure protein (purity higher than 90%) was collected by eluting in two fractions with 250 and 500 mM imidazole in buffer A, supplemented with 0.1% DDM. Production of MraY was monitored by a TLC-based Lipid II synthesis assay. The fractions were made into small aliquots and stored at −20 °C until further use.

UDP-MurNAc-Pentapeptide and [$^{15}N_2$]UMP Exchange Assay—BsMraY (14 nM) in 0.1% DDM, either free from C35-P or with C35-P at 100 μM, was incubated with UDP-MurNAc-pentapeptide (100 μM) and uridine-[$^{15}N_2$]5′-monophosphate (1 mM) for 16 h at room temperature in Tris-HCl buffer (pH 8.0) supplemented with Mg^{2+} (50 mM). The detergent was removed from the mixture using a C18 column before mass spectrometry measurements. Products were eluted in methanol/acetonitrile/water (2:2:1) and were analyzed with LC-MS to check whether the ^{15}N isotope was transferred from UMP to UDP-MurNAc-pentapeptide. LC-MS analysis was performed on an Exactive mass spectrometer (Thermo Fisher Scientific) coupled to a Dionex Ultimate 3000 autosampler and pump (Thermo Fisher Scientific). The MS operated in polarity-switching mode with spray voltages of 4.5 and 3.5 kV. Products were separated using a Sequant ZIC-pHILIC column (2.1 × 150 mm, 5 μm, guard column 2.1 × 20 mm, 5 μm; Merck). The flow rate was set at 150 μl/min, and products were separated using a linear gradient of acetonitrile and eluent A (20 mM $(NH_4)_2CO_3$, 0.1% NH_4OH in ULC/MS grade water (Biosolve)). Products were identified and quantified using LCquan software (Thermo Scientific) on the basis of exact mass within 5 ppm and further validated by concordance with retention times of UMP and UDP-MurNAc-pentapeptide standards.

TLC-based Lipid II Synthesis Assay—A TLC assay designed to test Lipid II synthesis was used to monitor MraY activity. In this assay, the MraY substrates C55-P (1 mM) and UDP-MurNAc-pentapeptide (100 μM), the MurG substrate UDP-GlcNAc (0.5 mM), $MgCl_2$ (6.7 mM), and pure MurG enzyme (20 nM) were mixed with Triton X-100 (0.5%) in Tris-HCl (100 mM, pH 8.0) buffer with a total volume of 75 μl. MraY-containing membrane fraction, BsMraY, or its mutant H289R was added last to initiate the synthesis. The reaction was quenched by the addition of pyridine-HAc (pH 4.2) to the mixture after incubation at room temperature for 1 h. Immediately thereafter, BuOH was added to the mixture, vortexed, and centrifuged briefly to induce phase separation. The upper layer was isolated and washed with 50 μl of water. After brief centrifugation, 10 μl of the upper layer was dried in a desiccator. The residue was taken up in $CHCl_3$/MeOH (1:1, v/v) and spotted on a silica gel plate. The plate was developed in $CHCl_3$/MeOH/H_2O/NH_3 (88:48:10:1 by volume). The lipids were subsequently visualized by iodide staining. C55-Lipid II was spotted as a reference.

Fluorescent Enhancement Assay and Kinetics Studies—MraY activity is determined using a fluorescent enhancement assay that was described earlier (28). Total volumes of 50 μl consisting of 25–400 μM C35-P, 15–100 μM UDP-MurNAc-pentapeptide-DNS, 200 mM Tris-HCl (pH 8.0), 0.5% Triton X-100, 50 mM $MgCl_2$, 100 mM KCl were mixed in 96-well plates. BsMraY (10 nM) was added with thorough mixing to initiate the reaction. The increase of fluorescence at λ_{em} = 510 nm (excitation wavelength λ_{ex} = 365 nm) was measured at 25 °C in a SpectraMax i3 microplate reader (Molecular Devices, Sunnyvale, CA). The increase of fluorescence was due to Lipid I formation as a result of the transfer of the dansyl label to a more hydrophobic environment (*i.e.* from the water-soluble UDP-MurNAc-pentapeptide to Lipid I embedded in a micelle). On the assumption that equilibrium had been reached under these conditions and using the known equilibrium constant (29) of 0.25 for the translocation reaction, the fluorescence signal (in relative fluorescent units) was converted into concentration of DNS-Lipid I (702,239.3 ± 0.3% relative fluorescent units/μM). Rate equations were derived for initial product formation in a random bi-bi mechanism (Fig. 1*A*) and for a ping-pong mechanism (Fig. 1*B*). Equation 1 for the random bi-bi mechanism turnover is as follows,

$$k = \frac{k_{cat}}{1 + \frac{K_m^{C35P}}{[C35\text{-}P]} + \frac{K_m^{UMpp}}{[UMpp\text{-}DNS]} + \frac{K_s^{C35P}}{[C35\text{-}P]} \times \frac{K_m^{UMpp}}{[UMpp\text{-}DNS]}} \quad \text{(Eq. 1)}$$

where K_m^{UMPP} gives the affinity for UDP-MurNAc-pentapeptide-DNS when a ternary complex is formed; $K_m^{C35\text{-}P}$ gives the affinity for C35-P when a ternary complex is formed; and $K_s^{C35\text{-}P}$ gives the affinity for C35-P when a binary complex is formed. The dependent constant K_s^{UMPP} (*i.e.* the affinity for UDP-MurNAc-pentapeptide-DNS when a binary complex is formed) is obtained from $K_s^{UMPP} = K_s^{C35\text{-}P} \times K_m^{UMPP}/K_m^{C35\text{-}P}$.

Equation 2 shows ping-pong mechanism turnover. At $t = 0$, [UMpp-DNS] = 0 and [Lipid I] = 0. Therefore, the steps represented by the *dotted arrows* in Fig. 1*B* are ignored.

$$k = \frac{k_{cat}}{1 + \frac{K_m^{UMpp}}{[UMpp\text{-}DNS]} + \frac{K_m^{C35\text{-}P}}{[C35\text{-}P]}} \quad \text{(Eq. 2)}$$

where $k_{cat} = k_1 \times k_2/(k_1 + k_2)$; $K_m^{UMPP} = K_s^{UMPP} \times k_2/(k_1 + k_2)$; and $K_m^{\#C35\text{-}P} = K_m^{C35\text{-}P} \times k_1/(k_1 + k_2)$.

Experimental data were fitted to Equation 1 or 2 using nonlinear regression (software JMP from SAS Inc. or GraphPad Prism).

Modeling of B. subtilis MraY—A structural model of BsMraY was built on the basis of the crystal structure data (Protein Data Bank code 4J72) of *A. aeolicus* MraY (AaMraY). The pairwise query-template alignment was obtained after an HHpred (30) search using the pdb70 database. In order to generate a global

sequence alignment, we enabled the "Realign with MAC algorithm" option and set the "MAC realignment threshold" to 0.0. The alignment was then used in MODELLER 9v12 (31) to generate 100 models, which were scored and ranked using the DOPE statistical potential (32). The lowest energy model provided the initial structure for the flexibility analysis with CONCOORD (33) and was also included in the docking simulations.

Modeling of Heptaprenyl Phosphate—The three-dimensional structure of C35-P was obtained using ChemBioDraw version 13.0 (generation of MOL file), OpenBabel (34) (conversion to Protein Data Bank), and Avogadro (35) (energy minimization with the GAFF force field). The resulting energy-minimized structure was then used in Antechamber/Acpype (36) with default options to generate parameters and topology files for HADDOCK (13). Given the natural flexibility of the C35-P molecule, we used HADDOCK (single-molecule refinement) to generate an ensemble of initial conformations for docking. During this process, the C35-P molecule was defined as fully flexible, and the explicit solvent refinement was carried out in DMSO, a lipid mimic. Due to the high temperature simulated annealing procedure and the parameter set we used, some of the resulting models were in conformations that, given our understanding of the (bio) chemistry of C35-P, we consider to be unrealistic. Hence, we manually selected five of the refined conformers based on their curvature, biasing toward mostly linear conformations, and overall stereochemistry for use in the docking simulations, instead of on the intramolecular energies alone.

Docking of Heptaprenyl Phosphate and B. subtilis MraY—The interaction between BsMraY and C35-P was modeled with HADDOCK (13) version 2.2 (37), using CNS (Crystallography and NMR System) version 1.3 (38) for structure calculations. Non-bonded interactions were calculated using the OPLS force field (39) using an 8.5 Å cut-off. The electrostatic interactions were modeled using a Coulomb potential including a shift function, whereas van der Waals interactions followed a Lennard-Jones potential using a switching function between 6.5 and 8.5 Å. The force field parameters for the magnesium ion were modified to match those defined by Allnér *et al.* (40), which describe the interaction of the divalent cation with phosphate ions more accurately. The partial charge of the ion was also reduced to +1 because docking with the full charge (+2) posed several challenges, in particular with the negatively charged phosphate ion of the substrate. The ion was also restrained to a coordinating residue on MraY (Asp-231) using unambiguous distance restraints to avoid drifting during the high temperature refinement stages. The HADDOCK score, a weighted sum of electrostatic, van der Waals, and restraint energy terms, was used to rank the models. The default desolvation energy term, derived for aqueous solution, was neglected because this system is embedded in a membrane. To force the molecules to obey the topology of the membrane, in the absence of an explicit bilayer model, we implemented a novel energy term in CNS, which we call "*z*-restraints" (not yet available in the standard 2.2 version of HADDOCK). These allow us to keep specific sections of a molecule in a particular subspace of the *z* (vertical) dimension (*e.g.* transmembrane helices and the hydrophobic tail of C35-P in the range of the thickness of the bilayer) and thus avoid meaningless orientations. The following BsMraY residues were restrained to a −20 Å/20 Å *z* boundary: 5–39, 72–90, 96–118, 130–146, 175–198, 202–228, 238–257, 266–305, and 336–355. These selections comprise α-helical segments and were based on the data shown by the OPM database for the AaMraY structure and on the calculations on the BsMraY model using the PPM2.0 server (15). All of C35-P was required to remain inside the defined *z* boundaries.

We first ran a docking simulation to sample possible binding surfaces of C35-P on MraY. This simulation used center-of-mass restraints together with a single unambiguous distance restraint with an upper limit of 7.5 Å between the terminal phosphor atom of C35-P and the imidazole nitrogen atoms of His-289 of BsMraY, in order to enforce the appropriate directionality of the C35-P molecule. The resulting models indicated a patch of hydrophobic residues in BsMraY TM5 (residues 174–199), which is close to reported catalytically important residues (Asn-168, Asn-171) but not a UDP-MurNAc-pentapeptide binding site (8), as a putative binding surface of C35-P. These TM5 residues were subsequently used as passive residues in a second round of docking simulations. For both simulations, we generated 10,000 models during the rigid body energy minimization stage, and the 400 best scoring models were selected for further refinement, which included semiflexible simulated annealing and explicit solvent (DMSO) molecular dynamics. The *z*-restraints were only active during the rigid body energy minimization stage. The final refined models were clustered using the fraction of common contacts algorithm (41) with a cut-off of 0.75, and each cluster was ranked by the average HADDOCK score of its four best members.

Flexibility Analysis of MraY—The conformational flexibility of monomeric BsMraY was probed using CONCOORD (version 2.1.2; available through the SBGRID consortium (42)) with the OPLS-AA (43) van der Waals parameters and default bond/angle parameters. As an input structure, we took the best-ranked model produced by MODELLER, judged by its DOPE score. Given the shortcomings of the homology model, namely the large insertions compared with the AaMraY structure, we fixed some parts of the model (residues 43–72 and 143–174) that would otherwise dominate the analysis. All other CONCOORD settings were left as default. The GROMACS (44) tool "trjconv" was used to extract representatives of the flexibility analysis.

Author Contributions—Y. L., E. B., and M. R. E. developed this study and designed the experiments; Y. L. carried out the production and activity study of MraY and its mutants; J. P. G. L. M. R. and A. M. J. J. B. carried out the modeling and docking studies; E. A. Z. and C. R. B. carried out mass spectrometry measurements and data analyses; M. H. carried out partial kinetics study and data analyses; and K. G. and E. S. synthesized C55-P and C35-P. All authors reviewed the results, revised the manuscript, and approved the final version of the manuscript.

Acknowledgments—We thank Dr. Tamimount Mohammadi for critically reading and commenting on the manuscript and Elisabete Moura for assistance during some experimental work. We also thank Prof. Ry Young for providing the ΔslyD BL21 strain.

References

1. Lloyd, A. J., Brandish, P. E., Gilbey, A. M., and Bugg, T. D. H. (2004) Phospho-*N*-acetyl-muramyl-pentapeptide translocase from *Escherichia coli*: catalytic role of conserved aspartic acid residues. *J. Bacteriol.* **186,** 1747–1757
2. Lovering, A. L., Safadi, S. S., and Strynadka, N. C. J. (2012) Structural perspective of peptidoglycan biosynthesis and assembly. *Annu. Rev. Biochem.* **81,** 451–478
3. Mihalyi, A., Jamshidi, S., Slikas, J., and Bugg, T. D. H. (2014) Identification of novel inhibitors of phospho-MurNAc-pentapeptide translocase MraY from library screening: isoquinoline alkaloid michellamine B and xanthene dye phloxine B. *Bioorg. Med. Chem.* **22,** 4566–4571
4. Winn, M., Goss, R. J. M., Kimura, K.-I., and Bugg, T. D. H. (2010) Antimicrobial nucleoside antibiotics targeting cell wall assembly: recent advances in structure-function studies and nucleoside biosynthesis. *Nat. Prod. Rep.* **27,** 279–304
5. Boyle, D. S., and Donachie, W. D. (1998) mraY is an essential gene for cell growth in *Escherichia coli*. *J. Bacteriol.* **180,** 6429–6432
6. Chung, B. C., Zhao, J., Gillespie, R. A., Kwon, D.-Y., Guan, Z., Hong, J., Zhou, P., and Lee, S.-Y. (2013) Crystal structure of MraY, an essential membrane enzyme for bacterial cell wall synthesis. *Science* **341,** 1012–1016
7. Bouhss, A., Crouvoisier, M., Blanot, D., and Mengin-Lecreulx, D. (2004) Purification and characterization of the bacterial MraY translocase catalyzing the first membrane step of peptidoglycan biosynthesis. *J. Biol. Chem.* **279,** 29974–29980
8. Al-Dabbagh, B., Henry, X., El Ghachi, M., Auger, G., Blanot, D., Parquet, C., Mengin-Lecreulx, D., and Bouhss, A. (2008) Active site mapping of MraY, a member of the polyprenyl-phosphate *N*-acetylhexosamine 1-phosphate transferase superfamily, catalyzing the first membrane step of peptidoglycan biosynthesis. *Biochemistry* **47,** 8919–8928
9. Ma, Y., Münch, D., Schneider, T., Sahl, H.-G., Bouhss, A., Ghoshdastider, U., Wang, J., Dötsch, V., Wang, X., and Bernhard, F. (2011) Preparative scale cell-free production and quality optimization of MraY homologues in different expression modes. *J. Biol. Chem.* **286,** 38844–38853
10. Brandish, P. E., Burnham, M. K., Lonsdale, J. T., Southgate, R., Inukai, M., and Bugg, T. D. H. (1996) Slow binding inhibition of phospho-*N*-acetylmuramyl-pentapeptide-translocase (*Escherichia coli*) by mureidomycin A. *J. Biol. Chem.* **271,** 7609–7614
11. Rodolis, M. T., Mihalyi, A., O'Reilly, A., Slikas, J., Roper, D. I., Hancock, R. E. W., and Bugg, T. D. H. (2014) Identification of a novel inhibition site in translocase MraY based upon the site of interaction with lysis protein e from bacteriophage ?X174. *ChemBioChem* **15,** 1300–1308
12. Huang, L. Y., Huang, S. H., Chang, Y. C., Cheng, W. C., Cheng, T. J., and Wong, C. H. (2014) Enzymatic synthesis of lipid II and analogues. *Angew. Chem. Int. Ed. Engl.* **53,** 8060–8065
13. Dominguez, C., Boelens, R., and Bonvin, A. M. J. J. (2003) HADDOCK: a protein-protein docking approach based on biochemical or biophysical information. *J. Am. Chem. Soc.* **125,** 1731–1737
14. Murakami, R., Muramatsu, Y., Minami, E., Masuda, K., Sakaida, Y., Endo, S., Suzuki, T., Ishida, O., Takatsu, T., Miyakoshi, S., Inukai, M., and Isono, F. (2009) A novel assay of bacterial peptidoglycan synthesis for natural product screening. *J. Antibiot.* **62,** 153–158
15. Lomize, M. A., Pogozheva, I. D., Joo, H., Mosberg, H. I., and Lomize, A. L. (2012) OPM database and PPM web server: resources for positioning of proteins in membranes. *Nucleic Acids Res.* **40,** D370–D376
16. Bouhss, A., Mengin-Lecreulx, D., Le Beller, D., and Van Heijenoort, J. (1999) Topological analysis of the MraY protein catalysing the first membrane step of peptidoglycan synthesis. *Mol. Microbiol.* **34,** 576–585
17. Al-Dabbagh, B., Mengin-Lecreulx, D., and Bouhss, A. (2008) Purification and characterization of the bacterial UDP-GlcNAc:undecaprenyl-phosphate GlcNAc-1-phosphate transferase WecA. *J. Bacteriol.* **190,** 7141–7146
18. Mihalyi, A. (2014) *Screening for Novel Inhibitors of Phospho-MurNAc-Pentapeptide Translocase MraY*. Ph.D. Thesis, University of Warwick
19. Chang, H. Y., Chou, C. C., Hsu, M. F., and Wang, A. H. J. (2014) Proposed carrier lipid-binding site of undecaprenyl pyrophosphate phosphatase from *Escherichia coli*. *J. Biol. Chem.* **289,** 18719–18735
20. Heydanek, M. G., Jr., Struve, W. G., and Neuhaus, F. C. (1969) On the initial stage in peptidoglycan synthesis. 3. Kinetics and uncoupling of phospho-*N*-acetylmuramyl-pentapeptide translocase (uridine 5′-phosphate). *Biochemistry* **8,** 1214–1221
21. Mendel, S., Holbourn, J. M., Schouten, J. A., and Bugg, T. D. H. (2006) Interaction of the transmembrane domain of lysis protein E from bacteriophage phiX174 with bacterial translocase MraY and peptidyl-prolyl isomerase SlyD. *Microbiology* **152,** 2959–2967
22. Tanaka, S., and Clemons, W. M., Jr. (2012) Minimal requirements for inhibition of MraY by lysis protein E from bacteriophage ΦX174. *Mol. Microbiol.* **85,** 975–985
23. Zheng, Y., Struck, D. K., Bernhardt, T. G., and Young, R. (2008) Genetic analysis of MraY inhibition by the phiX174 protein E. *Genetics* **180,** 1459–1466
24. Brandish, P. E., Kimura, K. I., Inukai, M., Southgate, R., Lonsdale, J. T., and Bugg, T. D. (1996) Modes of action of tunicamycin, liposidomycin B, and mureidomycin A: inhibition of phospho-*N*-acetylmuramyl-pentapeptide translocase from *Escherichia coli*. *Antimicrob. Agents Chemother.* **40,** 1640–1644
25. Swiezewska, E., Sasak, W., Mańkowski, T., Jankowski, W., Vogtman, T., Krajewska, I., Hertel, J., Skoczylas, E., and Chojnacki, T. (1994) The search for plant polyprenols. *Acta Biochim. Pol.* **41,** 221–260
26. Danilov, L. L., Druzhinina, T. N., Kalinchuk, N. A., Maltsev, S. D., and Shibaev, V. N. (1989) Polyprenyl phosphates: synthesis and structure-activity relationship for a biosynthetic system of *Salmonella anatum* O-specific polysaccharide. *Chem. Phys. Lipids* **51,** 191–203
27. Zheng, L., Baumann, U., and Reymond, J. L. (2004) An efficient one-step site-directed and site-saturation mutagenesis protocol. *Nucleic Acids Res.* **32,** e115
28. Stachyra, T., Dini, C., Ferrari, P., Bouhss, A., van Heijenoort, J., Mengin-Lecreulx, D., Blanot, D., Biton, J., and Le Beller, D. (2004) Fluorescence detection-based functional assay for high-throughput screening for MraY. *Antimicrob. Agents Chemother.* **48,** 897–902
29. Pless, D. D., and Neuhaus, F. C. (1973) Initial membrane reaction in peptidoglycan synthesis: lipid dependence of phospho-*n*-acetylmuramyl-pentapeptide translocase (exchange reaction). *J. Biol. Chem.* **248,** 1568–1576
30. Hildebrand, A., Remmert, M., Biegert, A., and Söding, J. (2009) Fast and accurate automatic structure prediction with HHpred. *Proteins* **77,** 128–132
31. Sali, A., and Blundell, T. L. (1993) Comparative protein modelling by satisfaction of spatial restraints. *J. Mol. Biol.* **234,** 779–815
32. Shen, M.-Y., and Sali, A. (2006) Statistical potential for assessment and prediction of protein structures. *Protein Sci.* **15,** 2507–2524
33. de Groot, B. L., van Aalten, D. M. F., Scheek, R. M., Amadei, A., Vriend, G., and Berendsen, H. J. C. (1997) Prediction of protein conformational freedom from distance constraints. *Proteins* **29,** 240–251
34. O'Boyle, N. M., Guha, R., Willighagen, E. L., Adams, S. E., Alvarsson, J., Bradley, J.-C., Filippov, I. V., Hanson, R. M., Hanwell, M. D., Hutchison, G. R., James, C. A., Jeliazkova, N., Lang, A. S., Langner, K. M., Lonie, D. C., *et al.* (2011) Open data, open source and open standards in chemistry: the Blue Obelisk five years on. *J. Cheminform.* **3,** 37
35. Hanwell, M. D., Curtis, D. E., Lonie, D. C., Vandermeersch, T., Zurek, E., and Hutchison, G. R. (2012) Avogadro: an advanced semantic chemical editor, visualization, and analysis platform. *J. Cheminform.* **4,** 17
36. Sousa da Silva, A. W., and Vranken, W. F. (2012) ACPYPE: antechamber Python parser interface. *BMC Res. Notes* **5,** 367
37. van Zundert, G. C., Rodrigues, J. P., Trellet, M., Schmitz, C., Kastritis, P. L., Karaca, E., Melquiond, A. S., van Dijk, M., de Vries, S. J., and Bonvin, A. M. (2016) The HADDOCK2.2 web server: user-friendly integrative modeling of biomolecular complexes. *J. Mol. Biol.* **428,** 720–725
38. Brunger, A. T. (2007) Version 1.2 of the Crystallography and NMR system. *Nat. Protoc.* **2,** 2728–2733
39. Jorgensen, W. L., and Tirado-Rives, J. (1988) The OPLS [optimized

potentials for liquid simulations] potential functions for proteins, energy minimizations for crystals of cyclic peptides and crambin. *J. Am. Chem. Soc.* **110,** 1657–1666
40. Allnér, O., Nilsson, L., and Villa, A. (2012) Magnesium ion-water coordination and exchange in biomolecular simulations. *J. Chem. Theory Comput.* **8,** 1493–1502
41. Rodrigues, J. P., Trellet, M., Schmitz, C., Kastritis, P., Karaca, E., Melquiond, A. S., and Bonvin, A. M. (2012) Clustering biomolecular complexes by residue contacts similarity. *Proteins* **80,** 1810–1817
42. Morin, A., Eisenbraun, B., Key, J., Sanschagrin, P. C., Timony, M. A., Ottaviano, M., and Sliz, P. (2013) Collaboration gets the most out of software. *Elife* **2,** e01456
43. Jorgensen, W. L., Maxwell, D. S., and Tirado-Rives, J. (1996) Development and testing of the OPLS all-atom force field on conformational energetics and properties of organic liquids. *J. Am. Chem. Soc.* **118,** 11225–11236
44. Hess, B., Kutzner, C., van der Spoel, D., and Lindahl, E. (2008) GRGMACS 4: algorithms for highly efficient, load-balanced, and scalable molecular simulation. *J. Chem. Theory Comput.* **4,** 435–447

New Insight into the Catalytic Mechanism of Bacterial MraY from Enzyme Kinetics and Docking Studies

Yao Liu, João P. G. L. M. Rodrigues, Alexandre M. J. J. Bonvin, Esther A. Zaal, Celia R. Berkers, Michal Heger, Katarzyna Gawarecka, Ewa Swiezewska, Eefjan Breukink and Maarten R. Egmond

J. Biol. Chem. 2016, 291:15057-15068.
doi: 10.1074/jbc.M116.717884 originally published online May 18, 2016
